



# In-Situ Cross-linked F- and P-Containing Solid Polymer Electrolyte for Long-Cycling and High-Safety Lithium Metal Batteries with Various Cathode Materials

Nuo Xu, Yang Zhao, Minghan Ni, Jie Zhu, Xingchen Song, Xingqi Bi, Jinping Zhang, Hongtao Zhang,\* Yanfeng Ma, Chenxi Li, and Yongsheng Chen\*

**Abstract:** The practical application of lithium metal batteries (LMBs) has been hindered by limited cycle-life and safety concerns. To solve these problems, we develop a novel fluorinated phosphate cross-linker for gel polymer electrolyte in high-voltage LMBs, achieving superior electrochemical performance and high safety simultaneously. The fluorinated phosphate cross-linked gel polymer electrolyte (FP-GPE) by *in-situ* polymerization method not only demonstrates high oxidation stability but also exhibits excellent compatibility with lithium metal anode. LMBs utilizing FP-GPE realize stable cycling even at a high cut-off voltage of 4.6 V (vs Li/Li<sup>+</sup>) with various high-voltage cathode materials. The LiNi<sub>0.6</sub>Co<sub>0.2</sub>Mn<sub>0.2</sub>O<sub>2</sub>|FP-GPE|Li battery exhibits an ultralong cycle-life of 1200 cycles with an impressive capacity retention of 80.1%. Furthermore, the FP-GPE-based batteries display excellent electrochemical performance even at practical conditions, such as high cathode mass loading (20.84 mgcm<sup>-2</sup>), ultrathin Li (20 μm), and a wide temperature range of -25 to 80 °C. Moreover, the first reported solid-state 18650 cylindrical LMBs have been successfully fabricated and demonstrate exceptional safety under mechanical abuse. Additionally, the industry-level 18650 cylindrical LiMn<sub>2</sub>O<sub>4</sub>|FP-GPE|Li<sub>4</sub>Ti<sub>5</sub>O<sub>12</sub> cells demonstrate a remarkable cycle-life of 1400 cycles. Therefore, the impressive electrochemical performance and high safety in practical batteries demonstrate a substantial potential of well-designed FP-GPE for large-scale industrial applications.

## Introduction

Lithium metal batteries (LMBs) are promising for next-generation energy storage system, owing to the high theoretical specific capacity (3860 mAhg<sup>-1</sup>) and the lowest redox potential (-3.04 V vs. the standard hydrogen electrode) of lithium metal anode (LMA).<sup>[1]</sup> Furthermore, LMBs assembled with high-voltage cathode materials can achieve even higher energy densities to meet the target of 500 Whkg<sup>-1</sup> setting by the evolving electric vehicle market.<sup>[2]</sup> Unfortunately, conventional organic liquid electrolytes (LEs) are unstable with LMA and high-voltage cathode materials.<sup>[3]</sup> These severe side reactions between LEs and electrodes can lead to the growth of Li dendrites and low Coulombic efficiency, potentially resulting in a short cycle-life and even safe hazards, such as combustion and explosion.<sup>[1a,4]</sup> The inferior cycling performance and associated safety concerns impede the practical deployment of LMBs.<sup>[5]</sup> Therefore, it is critical to develop high-voltage LMBs with long cycle-life, high safety and ease of large-scale fabrication for their practical applications.<sup>[6]</sup>

The gel polymer electrolytes (GPEs) for LMBs have been proposed to solve the problems of limited cycle-life and safety concerns.<sup>[7]</sup> Moreover, the *in-situ* polymerization process enables the fabrication of GPEs and the assembly of batteries at the same time, which is compatible with the existing battery industry system and has promising applications in large-scale production of solid-state LMBs.<sup>[8]</sup> Furthermore, cross-linking strategy is widely employed in GPEs to suppress Li dendrites growth by enhancing the mechanical strength of polymer matrices.<sup>[9]</sup> However, security issues persist due to the flammability of the polymer matrices and plasticizers. A practical solution is constructing GPEs with nonflammable polymer matrices by using flame-retardant cross-linkers, ensuring the safety of high-voltage LMBs.<sup>[10]</sup> Among various fire-retardant moieties, phosphate stands out for their low toxicity and superior ability to trap H<sup>•</sup> and OH<sup>•</sup>, and thus suppress combustion.<sup>[11]</sup> Nevertheless, the high reactivity between residual phosphate groups and LMA may impact the cycle-life of high-voltage LMBs.<sup>[12]</sup> Additionally, introducing F-containing groups into molecules is a well-established method to improve the oxidation stability towards high-voltage cathode materials and compatibility with LMA.<sup>[13]</sup> Consequently, introducing F-containing groups into the phosphate cross-linker to fabricate a F- and P-containing GPE polymer matrix may achieve

[\*] N. Xu, Y. Zhao, M. Ni, J. Zhu, X. Song, X. Bi, J. Zhang, H. Zhang, Y. Ma, C. Li, Y. Chen  
 The Centre of Nanoscale Science and Technology and Key Laboratory of Functional Polymer Materials, Institute of Polymer Chemistry, College of Chemistry, Nankai University, Tianjin 300071, China  
 E-mail: yschen99@nankai.edu.cn  
 htzhang@nankai.edu.cn

Y. Chen  
 State Key Laboratory of Elemento-Organic Chemistry, Nankai University, Tianjin, 300071, China  
 N. Xu, Y. Zhao, M. Ni, J. Zhu, X. Song, X. Bi, J. Zhang, H. Zhang, Y. Ma, C. Li, Y. Chen  
 Renewable Energy Conversion and Storage Center (RECAST), Nankai University, Tianjin 300071, China

superior electrochemical performance and high safety simultaneously.<sup>[14]</sup>

Herein, by introducing fluoroalkyl ( $-\text{CF}_2\text{CF}_2-$ ) into phosphate cross-linker (FP cross-linker), a novel cross-linked fluorinated phosphate-based GPE (FP-GPE) has been designed and synthesized for high-voltage LMBs. The incorporation of fluoroalkyl and phosphate segments synergistically enhances the fire-retardant efficiency of FP-GPE,<sup>[11b]</sup> thereby ensuring the high safety of the high-voltage LMBs. Additionally, the introduction of fluorinated segments endows FP-GPE with high electrochemical stability against high-voltage cathode materials and LMA, ensuring superior electrochemical performance of LMBs. The  $\text{LiNi}_{0.6}\text{Co}_{0.2}\text{Mn}_{0.2}\text{O}_2$  (NCM622)|FP-GPE|Li battery exhibits an ultralong cycle-life of 1200 cycles with an impressive capacity retention of 80.1 %, which is one of the best cycling performance in polymer electrolyte-based LMBs under comparable conditions so far. The FP-GPE also demonstrates compatibility with various high-voltage cathodes, enabling stable cycling even at a high charging cut-off voltage of 4.6 V. Furthermore, the FP-GPE-based LMBs display superior electrochemical performance under practical conditions, including high cathode mass loading ( $20.84 \text{ mg cm}^{-2}$ ), ultrathin Li ( $20 \mu\text{m}$ ), and a broad operating temperature range of  $-25$  to  $80^\circ\text{C}$ . Moreover, the FP-GPE-based solid-state 18650 cylindrical cells using LMA have been successfully fabricated for the first time, exhibiting a high capacity of 1.0 Ah and high-safety towards mechanical abuse. Additionally, the industry-level 18650 cylindrical  $\text{LiMn}_2\text{O}_4$ |FP-GPE| $\text{Li}_4\text{Ti}_5\text{O}_{12}$  cells demonstrate a remarkable cycle-life of 1400 cycles with a capacity retention of 70.5 %. This study paves the way for the development of LMBs with high electrochemical performance and high safety.

## Results and Discussion

### Design and Characterization of FP Cross-linker and FP-GPE

The design scheme of FP cross-linker is shown in Scheme 1a. To target a desired GPE, trimethylolpropane triacrylate (ETPTA) is chosen as the cross-linker to generate a cross-linked structure, contributing to excellent mechanical performance and the stability towards both high-voltage cathode materials and LMA.<sup>[15]</sup> However, the flammability of the polymer matrix is still a safety hazard. To enhance the safety of GPE, the phosphate moiety is introduced into the cross-linker and tri(acryloyloxyethyl) (TAEP) is obtained (the synthesis of TAEP is shown in SI). However, the high reactivity between phosphate and LMA may lead to unsatisfactory electrochemical performance. To simultaneously achieve excellent electrochemical performance and high safety, fluoroalkyl ( $-\text{CF}_2\text{CF}_2-$ ) is incorporated into the TAEP to enhance stability towards LMA and high-voltage cathodes. Therefore, the FP cross-linker has been designed, and the successful synthesis of FP-GPE is confirmed by proton, fluorine and carbon nuclear magnetic resonance spectroscopy ( $^1\text{H}$  NMR,  $^{19}\text{F}$  NMR,  $^{13}\text{C}$  NMR) and high-

resolution mass spectrum (HRMS) measurements, as shown in Figures S1–S3 (the synthesis of FP cross-linker is shown in SI). To fully utilize the advantages of FP cross-linker, vinylene carbonate (VC) has been selected as the monomer to fabricate FP-GPE, ensuring superior interfacial compatibility with both high-voltage cathodes and LMA.<sup>[16]</sup>

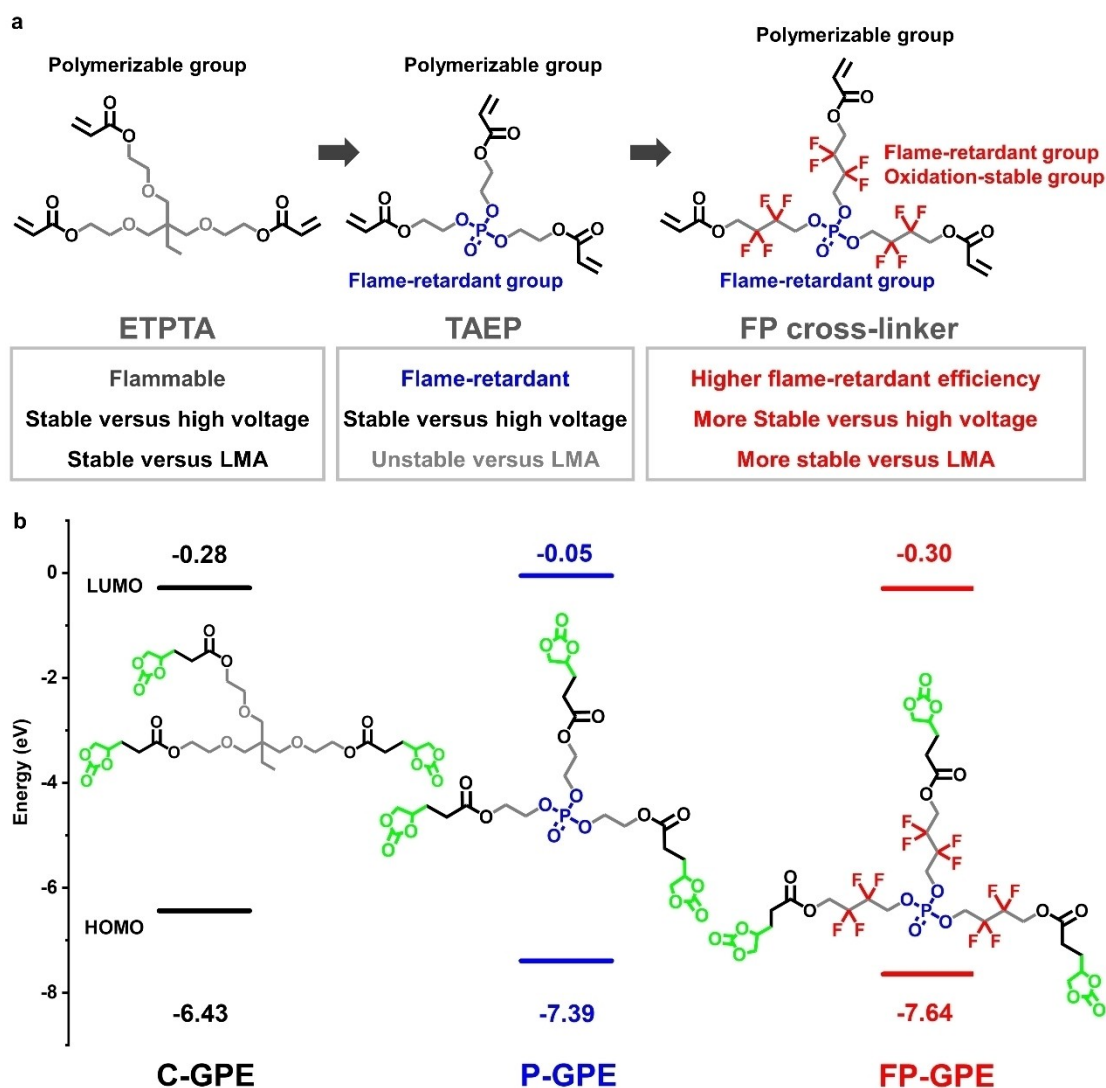
To evaluate the oxidation stability of the GPEs, the highest occupied molecular orbital (HOMO) and lowest unoccupied molecular orbital (LUMO) of the respective polymer segments are determined through density functional theory (DFT) simulations (Scheme 1b). As previously reported that fluorination can reduce the HOMO energy level,<sup>[17]</sup> the polymer matrix of FP-GPE exhibits a low HOMO energy level ( $-7.64 \text{ eV}$ ) compared to ETPTA cross-linked GPE (C-GPE) ( $-6.43 \text{ eV}$ ) and TAEP cross-linked GPE (P-GPE) ( $-7.39 \text{ eV}$ ), suggesting superior oxidation stability.

Consequently, C-GPE, P-GPE, and FP-GPE are prepared via *in-situ* polymerization of their respective cross-linkers. The liquid precursor transforms into gel after polymerization, and Fourier transform infrared spectrum (FT-IR) analysis of the polymer matrices confirm the copolymerization (Figures S4–S5).<sup>[18]</sup> Figure S6 and Video S1 illustrate that C-GPE is flammable upon contact with fire, while P-GPE and FP-GPE exhibit nonflammable properties, underscoring the enhanced safety achieved by TAEP and FP cross-linker. Therefore, FP-GPE exhibits the lowest HOMO and superior safety, aligning with our design concept.

### Electrochemical Performance of FP-GPE and LMBs

The electrochemical performance of FP-GPE is evaluated, with C-GPE and P-GPE as control electrolytes. Electrochemical floating analysis (EFA) is employed to study the long-term oxidation stability of FP-GPE. As shown in Figure 1a, no remarkable oxidation reaction in FP-GPE can be observed even under  $4.9 \text{ V}$  (*vs*  $\text{Li}/\text{Li}^+$ ), demonstrating an excellent stability under high voltage, which is desired in GPE for high-voltage LMBs. The temperature dependence of ionic conductivities for C-GPE, P-GPE, and FP-GPE has been studied from 298.15 to 313.15 K. As depicted in Figure 1b and Figure S7, the FP-GPE exhibits the highest ionic conductivity throughout the temperature range ( $4.45 \text{ mS cm}^{-1}$  at  $25^\circ\text{C}$ ). This superior ionic conductivity is attributed to the decreased activation energy of  $8.6 \text{ kJ mol}^{-1}$  for  $\text{Li}^+$  migration, indicating fast  $\text{Li}^+$  transport in FP-GPE, which is benefit for achieving high capacities and satisfactory rate performance.<sup>[10a,15b]</sup>

To evaluate the electrochemical performance of FP-GPE at high operating voltages, NCM622||Li coin cells are assembled and measured. Based on the high ionic conductivity, the NCM622|FP-GPE|Li battery demonstrates notable discharge capacities of 183.4, 180.8, 172.9, 165.1, 154.7 and  $134.3 \text{ mAh g}^{-1}$  at 0.1, 0.2, 0.5, 1, 2, and 5 C, respectively. Upon reverting to 0.5 C, the battery can still give a discharge capacity of  $172.6 \text{ mAh g}^{-1}$ , highlighting the great rate performance of FP-GPE-based high-voltage



**Scheme 1.** The design and structure of FP-GPE. (a) The design scheme of FP cross-linker. (b) The HOMO and LUMO energy levels of ETPTA, TAEP, and FP cross-linker.

LMBs. In contrast, LMBs based on C-GPE and P-GPE deliver lower discharge capacities of 146.1, 136.7 mAhg<sup>-1</sup> at 1 C under identical conditions (Figure S8). The cycling performance of NCM622|Li batteries are also evaluated. As illustrated in Figure 1c–1f, the NCM622|FP-GPE|Li battery exhibits an outstanding cycle-life of 1200 cycles with an impressive capacity retention of 80.1%, and 71.5% of the capacity retained even after 1500 cycles. This result is one of the most impressive cycling performances in polymer electrolyte-based LMBs in comparable conditions (Table S1). In contrast, the cycling stability of both NCM622|C-GPE|Li and NCM622|P-GPE|Li batteries is significantly inferior to that of the NCM622|FP-GPE|Li battery. Moreover, FP-GPE demonstrates ideal compatibility with various high-voltage cathode materials, exhibiting superior cycling performance compared to C-GPE and P-GPE-based LMBs. LiNi<sub>0.8</sub>Mn<sub>0.1</sub>Co<sub>0.1</sub>O<sub>2</sub> (NCM811)|FP-GPE|Li battery displays a discharge capacity of 181.8 mAhg<sup>-1</sup> and maintains a high capacity retention of 86.0% after 1000 cycles at 1 C (Fig-

ure 1g). Additionally, LiCoO<sub>2</sub>(LCO)|FP-GPE|Li battery exhibits a discharge capacity of 152.7 mAhg<sup>-1</sup> at 1 C, with a capacity retention of 79.7% after 1500 cycles (Figure S9). Furthermore, LiFePO<sub>4</sub> (LFP)|FP-GPE|Li battery demonstrates an exceptional capacity retention of 93.6% even after 4000 cycles at 2 C (Figure S10). In conclusion, FP-GPE-based LMBs assembled with various cathode materials, including NCM622, NCM811, LCO and LFP, demonstrate ultralong cycle-life with high capacity retentions (Table 1 and Table S2), thereby substantiating the impressive stability of FP-GPE.

#### Compatibility of FP-GPE with High-Voltage Cathode Materials and LMA

To investigate the excellent electrochemical performance of FP-GPE in high-voltage LMBs, the cathode electrolyte interphase (CEI) and solid electrolyte interphase (SEI) are

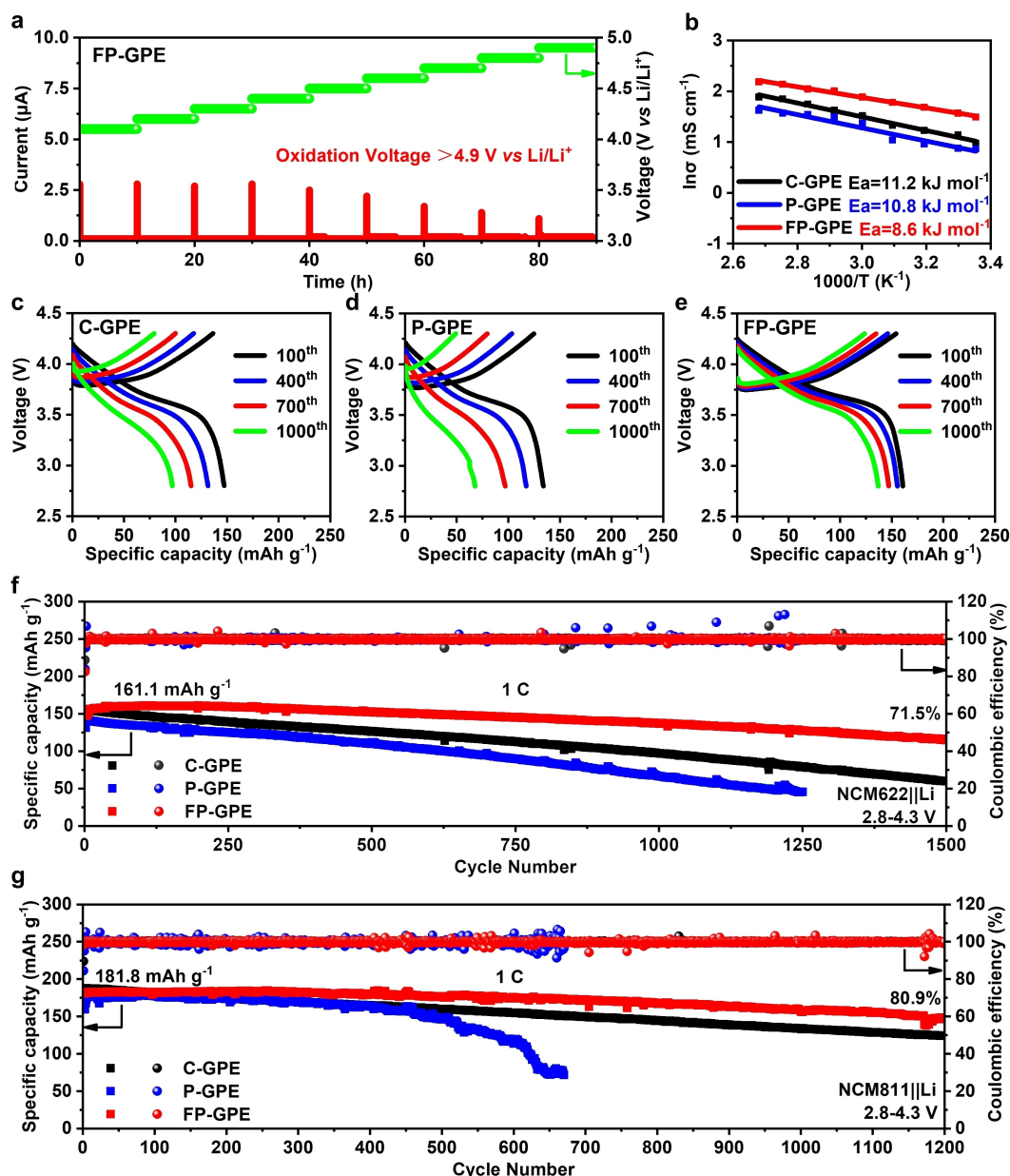


**Figure 1.** Electrochemical performance. (a) Electrochemical floating analysis of FP-GPE. (b) Temperature-dependent ionic conductivities of C-GPE, P-GPE, and FP-GPE. Typical charge–discharge curves of NCM622 || Li batteries with (c) C-GPE, (d) P-GPE and (e) FP-GPE in the voltage range of 2.8–4.3 V at 25 °C under 1 C. (f) Long-cycling performance of NCM622 || Li batteries with C-GPE, P-GPE and FP-GPE in the voltage range of 2.8–4.3 V at 25 °C under 1 C. (g) Long-cycling performance of NCM811 || Li batteries with C-GPE, P-GPE and FP-GPE in the voltage range of 2.8–4.3 V at 25 °C under 1 C.

characterized. From transmission electron microscope (TEM) images of cycled NCM622 cathodes (Figure 2a–2c and Figure S11), a uniform CEI with a thickness of only about 5 nm is observed in FP-GPE, and the layered-phase structure is retained well in NCM622 after cycling. These evidences underscore the high stability of FP-GPE with high-voltage cathode.<sup>[19]</sup> In contrast, the uneven and thick CEI layers formed in both P-GPE (about 8 nm) and C-GPE (about 19 nm) indicate the severe side reactions between the high-voltage cathode and electrolytes.<sup>[20]</sup> The X-ray photoelectron spectroscopy (XPS) analysis is carried out to

identify the component of CEI (Figure S11). Compared to C-GPE and P-GPE, the CEI formed in FP-GPE is inorganic-rich with a high content of  $\text{Li}_x\text{PO}_y\text{F}_z$  (687 eV)<sup>[21]</sup> and LiF (685 eV).<sup>[22]</sup>  $\text{Li}_x\text{PO}_y\text{F}_z$  can scavenge dissolved transition metal ions and impede their migration, while LiF-rich CEI exhibits a low electronic conductivity and avoids further decomposition of FP-GPE.<sup>[13c,23]</sup> In summary, a thin, uniform and inorganic-rich CEI forms between FP-GPE and NCM622 cathode, contributing to the outstanding electrochemical performance of high-voltage LMBs.

**Table 1:** Cycling performance of LMBs based on FP-GPE.

Cathode material	Voltage range (V)	Current density	Specific capacity ( $\text{mAh g}^{-1}$ )	Cycle number	Capacity retention
NCM622	2.8–4.3	1C	161.1	1000	85.0%
				1200	80.1%
				1500	71.5%
NCM811	2.8–4.3	1C	181.8	1000	86.0%
				1200	80.9%
				1000	88.9%
LCO	2.8–4.3	1C	152.7	1200	86.0%
				1500	79.7%
				1000	98.9%
LFP	2.5–4.0	2C	141.7	3000	98.0%
				4000	93.6%

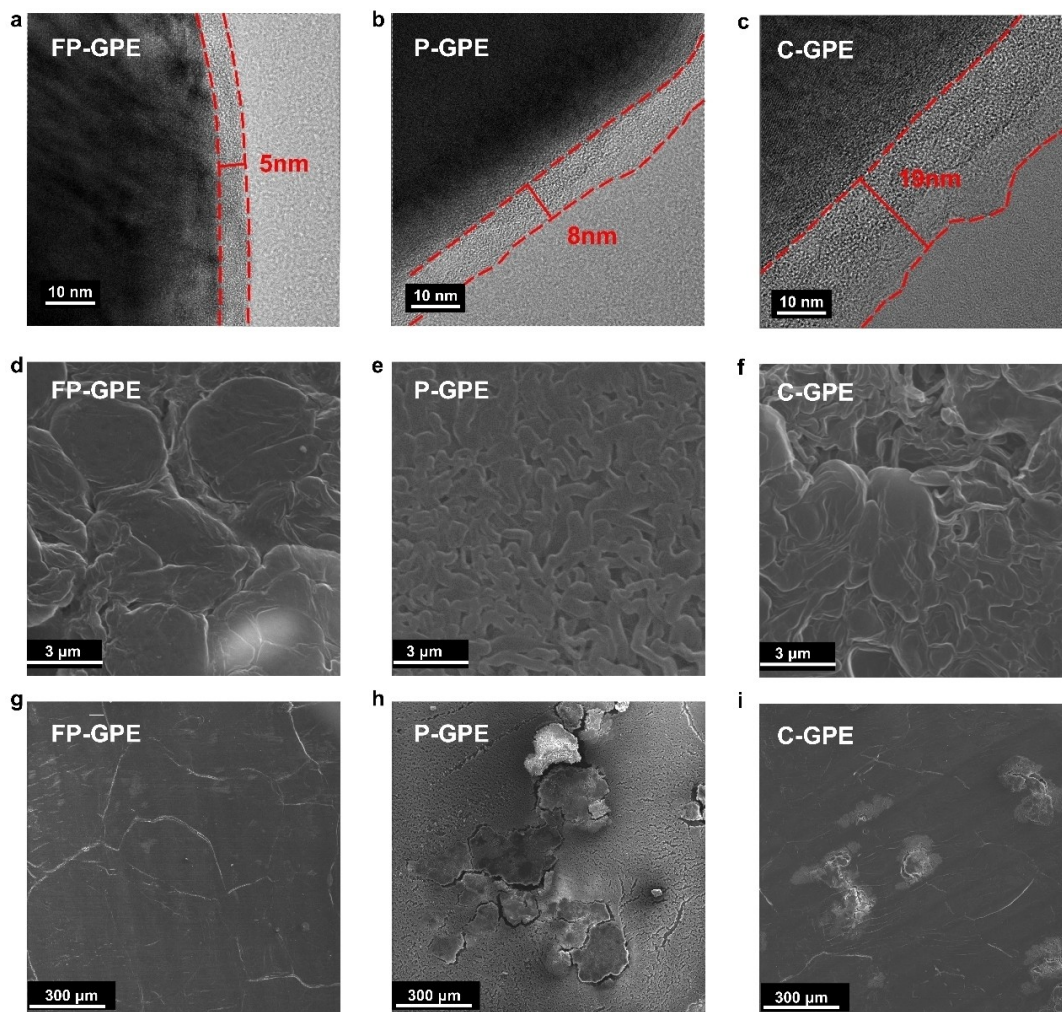


**Figure 2.** The characterization of CEI and SEI. TEM images of cycled NCM622 cathodes in NCM622 || Li batteries after 50 cycles with (a) FP-GPE, (b) P-GPE, and (c) C-GPE in the voltage range of 2.8–4.3 V at 25 °C under 1 C. SEM images of cycled Li in Li || Li symmetric cells after 50 cycles with (d, g) FP-GPE, (e, h) P-GPE, and (f, i) C-GPE at a current density of  $0.1 \text{ mAcm}^{-2}$  and a capacity of  $0.1 \text{ mAh cm}^{-2}$  at 25 °C.

The stability between GPE and LMA is equally crucial in high-voltage LMBs.<sup>[4c]</sup> The Li || Li symmetric cells are assembled to evaluate the stability of LMA in different GPEs (Figure S12). FP-GPE displays a high critical current density (CCD) of  $4.5 \text{ mAcm}^{-2}$ , and Li || Li symmetric cell exhibits stable overpotential for 700 h, demonstrating high

stability to LMA (Figure S13). By contrast, P-GPE-based symmetric cell exhibits a large overpotential and a poor cycle-life ( $\sim 150 \text{ h}$ ), indicating high reactivity between LMA and P-GPE.<sup>[12,24]</sup> The prolonged cycle-life of the FP-GPE-based Li || Li symmetric cell demonstrates the enhanced stability against LMA achieved by incorporating fluoroalkyl

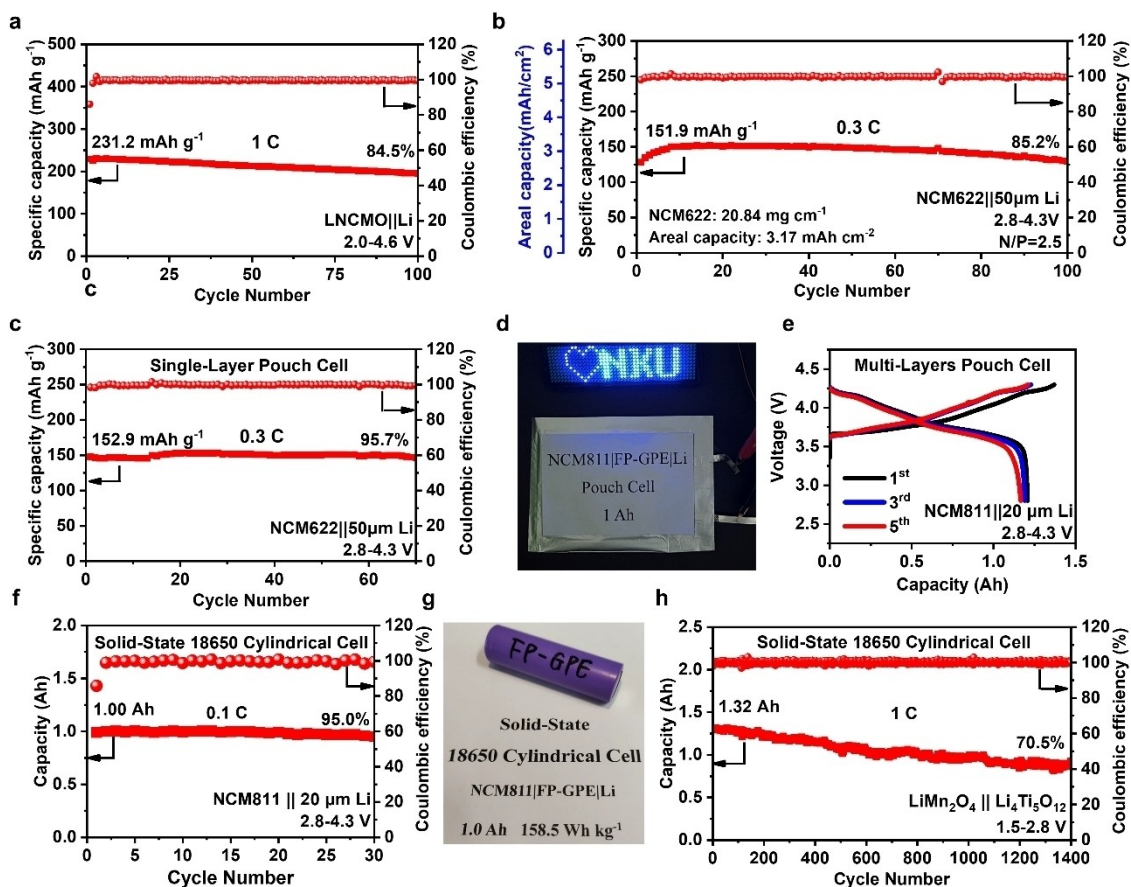


**Figure 3.** Cycling performance of FP-GPE-based lithium batteries. (a) Cycling performance of the LNCMO|FP-GPE|Li battery in the voltage range of 2.0–4.6 V at 25 °C under 1 C. (b) Cycling performance of the NCM622|FP-GPE|Li full cell in the voltage range of 2.8–4.3 V at 25 °C under 0.3 C. (c) Cycling performance of the single-layer NCM622|FP-GPE|Li pouch cell in the voltage range of 2.8–4.3 V at 25 °C under 0.3 C. (d) Digital photo of the 1 Ah NCM811|FP-GPE|Li pouch cell. (e) Typical charge–discharge curves of 1 Ah NCM811|FP-GPE|Li pouch cell in the voltage range of 2.8–4.3 V at 25 °C under 0.1 C. (f) Cycling performance of the NCM811|Li cylindrical cell with FP-GPE in the voltage range of 2.8–4.3 V at 25 °C under 0.1 C. (g) Digital photo of FP-GPE-based solid-state 18650 cylindrical cell. (h) Cycling performance of the 18650 cylindrical  $\text{LiMn}_2\text{O}_4$ | $\text{Li}_4\text{Ti}_5\text{O}_{12}$  cell with FP-GPE in the voltage range of 1.5–2.8 V at 25 °C under 1 C.

( $-\text{CF}_2-\text{CF}_2$ ) groups into TAEP. The morphology of cycled Li in Li||Li symmetric cells further reveals distinct difference. A uniform and dense morphology with large-grains Li deposition is realized in FP-GPE (Figure 2d and 2g), indicating the excellent stability towards LMA.<sup>[25]</sup> In contrast, for P-GPE, the fiber-like Li deposition morphology with many cracks and mossy Li structures can be clearly observed on the surface of LMA (Figure 2e and 2h), contributing to the short cycle-life of batteries.<sup>[2a]</sup> In addition, scanning electron microscopy (SEM) images for C-GPE also displays inferior Li deposition morphology (Figure 2f and 2i). Compared to P-GPE, XPS analysis of cycled Li in FP-GPE reveals a lower content of  $\text{Li}_3\text{PO}_4$ , attributed to the phosphate decomposition, illustrating the improved stability to LMA through the incorporation of fluoroalkyl groups into phosphate (Figure S14).<sup>[10a]</sup> Moreover, an inorganic-rich SEI layer forms in FP-GPE with a large amount of  $\text{LiF}$  and  $\text{Li}_x\text{PO}_y\text{F}_z$ , enhancing the strength of LMA surface and facilitating the homogeneous  $\text{Li}^+$  deposition.<sup>[26]</sup> The excellent electrochemical stability and interphase morphol-

ogy between FP-GPE and electrodes ensure the outstanding cycling performance of FP-GPE-based high-voltage LMBs.

#### Stable Operation of High-Voltage LMBs and Full Cells

Raising the charging cut-off voltage of LMBs is a promising method to increase their energy density.<sup>[27]</sup> The electrochemical performance of FP-GPE-based LMBs is further tested at elevated charging cut-off voltages at a rate of 1 C. At the voltage of 4.5 V, the LMBs with NCM622 and NCM811 cathode materials exhibit excellent cycling performance with increased specific capacities (Figure S15–S16). Notably, LCO|FP-GPE|Li battery delivers a high specific capacity of  $184.0 \text{ mAh g}^{-1}$  with a high retention of 82.1% even after 500 cycles (Figure S17).

Moreover, Li-rich Mn-based layered oxides (LLO) are promising candidates for next-generation cathode materials for their high specific capacity (over  $250 \text{ mAh g}^{-1}$ ) and high average discharge voltage (3.5 V).<sup>[28]</sup> However, limited by the narrow electrochemical stability windows, only a few

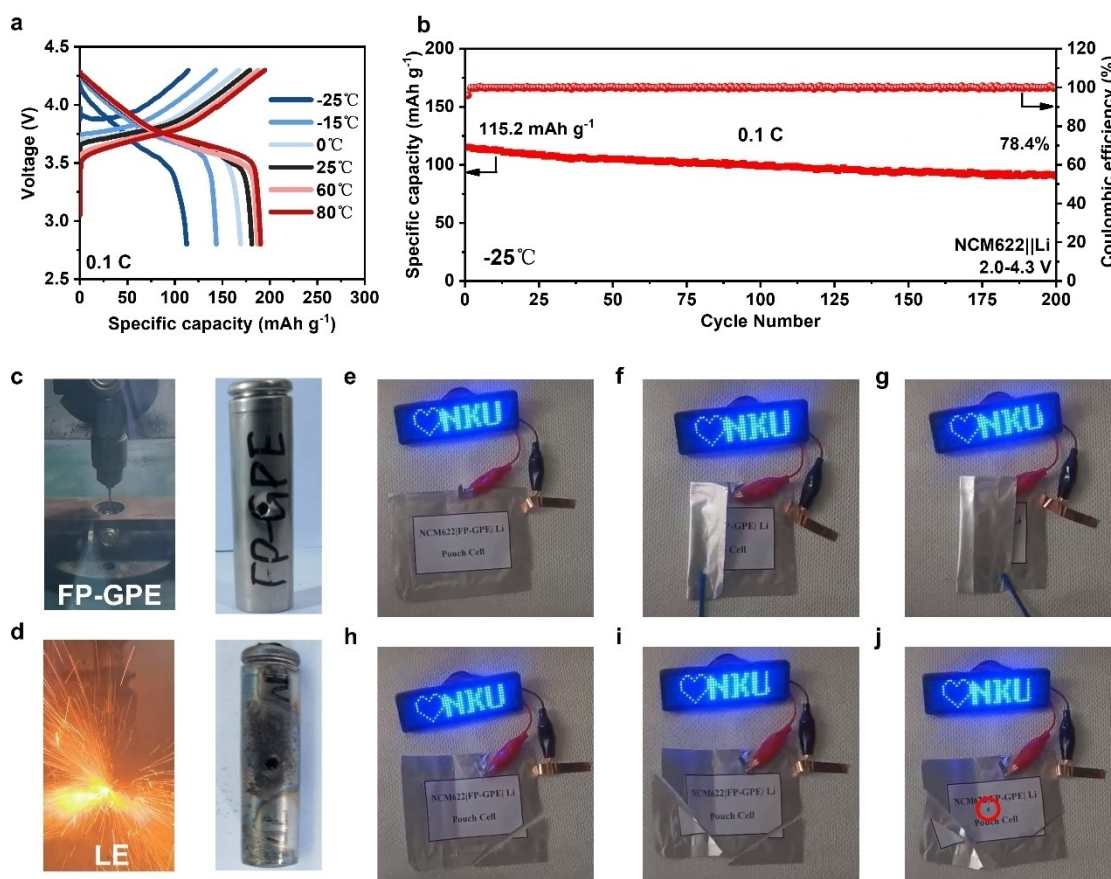


**Figure 4.** Safety tests of FP-GPE and batteries with FP-GPE. (a) Typical charge–discharge curves of NCM622 || Li batteries with FP-GPE in the voltage range of 2.8–4.3 V at different temperatures under 0.1 C. (b) Cycling performance of the NCM622 | FP-GPE | Li battery in the voltage range of 2.8–4.3 V at  $-25^{\circ}\text{C}$  under 0.1 C. Nail test of NCM811 || Li cylindrical cell with (c) FP-GPE and (d) LE. An LED powered by a NCM622 || Li pouch cell with FP-GPE e) before and after f, g) bending, h, i) cutting, j) nail tests.

GPEs are compatible with LLO cathodes.<sup>[29]</sup> While, owing to the excellent oxidation stability of FP-GPE,  $\text{Li}_{1.2}\text{Ni}_{0.13}\text{Co}_{0.13}\text{Mn}_{0.54}\text{O}_2$  (LNCMO) | FP-GPE | Li battery displays a high specific capacity of  $231.2\text{ mAh g}^{-1}$  at 1 C and a high capacity retention of 84.5 % after 100 cycles under a charging cut-off voltage of 4.6 V (Figure 3a). The FP-GPE-based LMBs assembled with NCM622, NCM811 and LCO also exhibit superior cycling stability at 4.6 V (Figure S18). As depicted in Figures S19–S23, the specific capacities of FP-GPE-based LMBs with different cathode materials noticeably increase with the raising voltage, indicating the potential for achieving higher energy density.

The remarkable electrochemical performance of FP-GPE enables its practical application scenarios. The Li metal full cells with low N/P ratios are assembled using ultrathin Li foil ( $50\ \mu\text{m}$ ) and high mass-loading NCM622 (8.49 and  $20.84\text{ mg cm}^{-2}$ ) as electrodes. Figure S24 shows that the NCM622 | FP-GPE | Li full cell can cycle steadily for 300 cycles at 1 C with a cathode mass-loading of  $8.49\text{ mg cm}^{-2}$ . Increasing the cathode mass-loading up to  $20.84\text{ mg cm}^{-2}$ , the NCM622 | FP-GPE | Li full cell (with a low N/P ratio of 2.5) delivers a high areal capacity of  $3.17\text{ mAh cm}^{-2}$  with a capacity retention of 85.2 % after 100 cycles at 0.3 C (Figure 3b).

Furthermore, the NCM622 | FP-GPE | Li ( $50\ \mu\text{m}$ ) pouch cells exhibit a capacity retention of 95.7 % after 70 cycles (Figure 3c). The multi-layers NCM811 | FP-GPE | Li pouch cells are also fabricated and display a capacity of 1.2 Ah (Figure 3d and 3e). More importantly, the first reported solid-state 18650 cylindrical LMBs have been successfully fabricated using FP-GPE with NCM811 cathode and Li metal anode (N/P ratio = 2.5). The FP-GPE-based 18650 cylindrical LMBs deliver a high capacity of 1.0 Ah, a high energy density of  $158.5\text{ Wh kg}^{-1}$  ( $227.2\text{ Wh kg}^{-1}$  without considering the packing material, Table S3) and a high capacity retention of 95.0 % after 30 cycles (Figure 3f), superior to the performance with commercial LE (1 M  $\text{LiPF}_6$  in  $\text{DMC}:\text{EC}:\text{EMC}=1:1:1$  in volume) (Figure S25). Additionally, the FP-GPE-based industrial-level solid-state 18650 cylindrical lithium-ion batteries ( $\text{LiMn}_2\text{O}_4$  |  $\text{Li}_4\text{Ti}_5\text{O}_{12}$ ) also demonstrate an outstanding cycling stability of 1400 cycles with a high retention of up to 70.5 % (Figure 3h). The successful fabrication and the impressive electrochemical performance of both pouch and 18650 cylindrical cells demonstrate that the well-designed FP-GPE possesses significant potential for large-scale industrial applications.

**Electrochemical Performance and Safety of FP-GPE-Based LMBs under Harsh Conditions**

To further validate the electrochemical performance and safety of FP-GPE-based high-voltage LMBs under harsh conditions, NCM622|FP-GPE|Li batteries are assembled and cycled at different temperatures. The FP-GPE-based batteries exhibit high specific capacities and cycling stability across a broad temperature range of  $-25$  to  $80^{\circ}\text{C}$  (Figure 4a and Figure S26). At  $60^{\circ}\text{C}$ , the LMB with FP-GPE displays a high discharge capacity of  $187.0\text{ mAh g}^{-1}$  at  $0.1\text{ C}$  and a high retention of  $87.5\%$  after 150 cycles. While the capacities of batteries with P-GPE and C-GPE decay rapidly. Notably, even at a low temperature of  $-25^{\circ}\text{C}$ , the FP-GPE demonstrates a high ionic conductivity of  $1.12\text{ mS cm}^{-1}$  (Figure S27). As a result, the NCM622|FP-GPE|Li battery exhibits an initial discharge capacity of  $115.2\text{ mAh g}^{-1}$  and an outstanding capacity retention of  $78.4\%$  after 200 cycles (Figure 4b).

Furthermore, both 18650 cylindrical and pouch LMBs using FP-GPE possess excellent safety in mechanical abuse tests. After being penetrated by a metal nail, the FP-GPE-based solid-state 18650 cylindrical NCM811||Li cells exhibit excellent safety without electrolyte leakage or combustion (Figure 4c and Video S2), due to the condensed character and the nonflammability of the F- and P- containing polymer matrices. In sharp contrast, the LE-based NCM811||Li 18650 cylindrical cells burst into flame (Figure 4d and Video S3). Additionally, the NCM622||Li pouch cell assembled with FP-GPE can still power the light emitting diode (LED) even after bending, cutting and nail-penetration tests (Figure 4e–4j and Video S4), demonstrating its high safety and flexibility.

**Conclusion**

In summary, by introducing fluoroalkyl ( $-\text{CF}_2\text{CF}_2-$ ) in to phosphate cross-linker, we have designed and synthesized a FP cross-linker for high-voltage LMBs. Due to the rational design of FP cross-linker, the *in-situ* polymerized FP-GPE demonstrates high oxidation stability ( $>4.9\text{ V vs Li/Li}^+$ ), excellent compatibility with various high-voltage cathodes, superior cycling stability and high safety. The NCM622|FP-GPE|Li battery exhibits an ultralong cycle-life of 1200 cycles with a high retention of  $80.1\%$ . Furthermore, FP-GPE facilitates LMBs to achieve exceptional electrochemical performance even under practical conditions, including high cathode mass loading ( $20.84\text{ mg cm}^{-2}$ ) and ultrathin Li ( $20\text{ }\mu\text{m}$ ), extreme temperature conditions ( $-25$  to  $80^{\circ}\text{C}$ ). Moreover, 1 Ah pouch cells and 18650 cylindrical cells assembled with FP-GPE display outstanding electrochemical performance with high safety towards mechanical abuse. Therefore, our work paves the way for the development of high-performance, high-voltage, and high-safety LMBs.

**Supporting Information**

Supporting Information is available from the Wiley Online Library or from the author.

**Acknowledgements**

The authors gratefully acknowledge the financial support from The National Key R&D Program of China (2020YFA0711500), National Natural Science Foundation of China (NSFC, 52090034).

**Conflict of Interest**

The authors declare no conflict of interest.

**Data Availability Statement**

The data that support the findings of this study are available in the supplementary material of this article.

**Keywords:** lithium metal battery · *in-situ* cross-linked · gel polymer electrolyte · long cycle-life · high safety

- [1] a) X. Ren, L. Zou, X. Cao, M. H. Engelhard, W. Liu, S. D. Burton, H. Lee, C. Niu, B. E. Matthews, Z. Zhu, C. Wang, B. W. Arey, J. Xiao, J. Liu, J.-G. Zhang, W. Xu, *Joule* **2019**, *3*, 1662–1676; b) X. Sun, X. Zhang, Q. Ma, X. Guan, W. Wang, J. Luo, *Angew. Chem. Int. Ed.* **2020**, *59*, 6665–6674; c) J. Zhu, J. Zhang, R. Zhao, Y. Zhao, J. Liu, N. Xu, X. Wan, C. Li, Y. Ma, H. Zhang, Y. Chen, *Energy Storage Mater.* **2023**, *57*, 92–101; d) X. R. Chen, B. C. Zhao, C. Yan, Q. Zhang, *Adv. Mater.* **2021**, *33*, 2004128.
- [2] a) Y. Zhang, Y. Wu, H. Li, J. Chen, D. Lei, C. Wang, *Nat. Commun.* **2022**, *13*, 1297; b) Z. Wang, H. Zhang, J. Xu, A. Pan, F. Zhang, L. Wang, R. Han, J. Hu, M. Liu, X. Wu, *Adv. Funct. Mater.* **2022**, *32*, 2112598; c) Y. Xu, K. Dong, Y. Jie, P. Adelhelm, Y. Chen, L. Xu, P. Yu, J. Kim, Z. Kochovski, Z. Yu, W. Li, J. LeBeau, Y. Shao-Horn, R. Cao, S. Jiao, T. Cheng, I. Manke, Y. Lu, *Adv. Energy Mater.* **2022**, *12*, 2200398; d) J. Liu, Z. Bao, Y. Cui, E. J. Dufek, J. B. Goodenough, P. Khalifah, Q. Li, B. Y. Liaw, P. Liu, A. Manthiram, Y. S. Meng, V. R. Subramanian, M. F. Toney, V. V. Viswanathan, M. S. Whittingham, J. Xiao, W. Xu, J. Yang, X.-Q. Yang, J.-G. Zhang, *Nat. Energy* **2019**, *4*, 180–186.
- [3] Z. Wen, W. Fang, F. Wang, H. Kang, S. Zhao, S. Guo, G. Chen, *Angew. Chem. Int. Ed.* **2024**, e202314876.
- [4] a) J. Qian, W. A. Henderson, W. Xu, P. Bhattacharya, M. Engelhard, O. Borodin, J.-G. Zhang, *Nat. Commun.* **2015**, *6*, 6362; b) S. Chen, J. Fan, Z. Cui, L. Tan, D. Ruan, X. Zhao, J. Jiang, S. Jiao, X. Ren, *Angew. Chem. Int. Ed.* **2023**, *62*, e202219310; c) K. Qin, K. Holguin, M. Mohammadiroudbari, J. Huang, E. Y. S. Kim, R. Hall, C. Luo, *Adv. Funct. Mater.* **2021**, *31*, 2009694; d) J. Li, Y. Cai, H. Wu, Z. Yu, X. Yan, Q. Zhang, T. Z. Gao, K. Liu, X. Jia, Z. Bao, *Adv. Energy Mater.* **2021**, *11*, 2003239.
- [5] S. Chai, Z. Chang, Y. Zhong, Q. He, Y. Wang, Y. Wan, M. Feng, Y. Hu, W. Li, W. Wei, A. Pan, *Adv. Funct. Mater.* **2023**, *33*, 2300425.

- [6] Y. Zhang, L. Yu, X. D. Zhang, Y. H. Wang, C. P. Yang, X. L. Liu, W. P. Wang, Y. Zhang, X. T. Li, G. Li, S. Xin, Y. G. Guo, C. L. Bai, *Sci. Adv.* **2023**, *9*, eade5802.
- [7] a) X. Cheng, J. Pan, Y. Zhao, M. Liao, H. Peng, *Adv. Energy Mater.* **2017**, *8*, 1702184; b) C. Ma, W. Cui, X. Liu, Y. Ding, Y. Wang, *InfoMat* **2021**, *4*, e12232; c) Y. Han, Y. Zhou, J. Zhu, Z. Sun, L. Xu, C. Li, Y. Ma, H. Zhang, Y. Chen, *Sci. China Mater.* **2020**, *63*, 2344–2350.
- [8] a) B. H. Zhang, Y. Wu, Y. L. Hou, J. Z. Chen, Z. Ma, D. L. Zhao, *Small* **2023**, *20*, 2305322; b) V. Vijayakumar, B. Anothumakkool, S. Kurungot, M. Winter, J. R. Nair, *Energy Environ. Sci.* **2021**, *14*, 2708–2788; c) L. Qi, W. Li, H. Xiangming, *Adv. Energy Mater.* **2023**, *13*, 2300798; d) Q. Zhao, X. Liu, S. Stalin, K. Khan, L. A. Archer, *Nat. Energy* **2019**, *4*, 365–373.
- [9] a) H. Yang, M. X. Jing, H. P. Li, W. Y. Yuan, B. Deng, Q. Y. Liu, B. W. Ju, X. Y. Zhang, S. Hussain, X. Q. Shen, X. H. Yan, *Chem. Eng. J.* **2021**, *421*, 129710; b) Q. Zhang, X. Liu, H. Li, Z. J. Guo, T. F. Bian, X. B. Zhu, N. N. Zhan, Y. Zhao, *Small* **2022**, *18*, 2106395; c) M. Shen, Z. Wang, D. Cheng, H. Cheng, H. Xu, Y. Huang, *eTransportation* **2023**, *18*, 100264.
- [10] a) Y. F. Meng, D. Zhou, R. L. Liu, Y. Tian, Y. F. Gao, Y. Wang, B. Sun, F. Y. Kang, M. Armand, B. H. Li, G. X. Wang, D. Aurbach, *Nat. Energy* **2023**, *8*, 1023–1033; b) T. Zhu, G. Liu, D. Chen, J. Chen, P. Qi, J. Sun, X. Gu, S. Zhang, *Energy Storage Mater.* **2022**, *50*, 495–504; c) J. Zheng, Y. Sun, W. Li, X. Feng, W. Chen, Y. Zhao, *ACS Appl. Mater. Interfaces* **2021**, *13*, 25024–25035; d) X. Mu, X. Li, C. Liao, H. Yu, Y. Jin, B. Yu, L. Han, L. Chen, Y. Kan, L. Song, Y. Hu, *Adv. Funct. Mater.* **2022**, *32*, 2203006.
- [11] a) P. Jaumaux, J. Wu, D. Shanmukaraj, Y. Wang, D. Zhou, B. Sun, F. Kang, B. Li, M. Armand, G. Wang, *Adv. Funct. Mater.* **2020**, *31*, 2008644; b) K. Deng, Q. Zeng, D. Wang, Z. Liu, G. Wang, Z. Qiu, Y. Zhang, M. Xiao, Y. Meng, *Energy Storage Mater.* **2020**, *32*, 425–447.
- [12] S. Tan, J. Yue, Y. F. Tian, Q. Ma, J. Wan, Y. Xiao, J. Zhang, Y. X. Yin, R. Wen, S. Xin, Y. G. Guo, *Energy Storage Mater.* **2021**, *39*, 186–193.
- [13] a) Z. Yu, H. Wang, X. Kong, W. Huang, Y. Tsao, D. G. Mackanic, K. Wang, X. Wang, W. Huang, S. Choudhury, Y. Zheng, C. V. Amanchukwu, S. T. Hung, Y. Ma, E. G. Lomeli, J. Qin, Y. Cui, Z. Bao, *Nat. Energy* **2020**, *5*, 526–533; b) Q. Zheng, Y. Yamada, R. Shang, S. Ko, Y. Lee, K. Kim, E. Nakamura, A. Yamada, *Nat. Energy* **2020**, *5*, 291–298; c) L. Tang, B. Chen, Z. Zhang, C. Ma, J. Chen, Y. Huang, F. Zhang, Q. Dong, G. Xue, D. Chen, C. Hu, S. Li, Z. Liu, Y. Shen, Q. Chen, L. Chen, *Nat. Commun.* **2023**, *14*, 2301.
- [14] J. A. Choi, Y. Kang, H. Shim, D. W. Kim, E. Cha, D. W. Kim, *J. Power Sources* **2010**, *195*, 6177–6181.
- [15] a) J. Li, T. Zhang, X. Hui, R. Zhu, Q. Sun, X. Li, L. Yin, *Adv. Sci.* **2023**, *10*, 2300226; b) A. Wang, S. Geng, Z. Zhao, Z. Hu, J. Luo, *Adv. Funct. Mater.* **2022**, *33*, 2201861.
- [16] a) J. Zhang, J. Yang, T. Dong, M. Zhang, J. Chai, S. Dong, T. Wu, X. Zhou, G. Cui, *Small* **2018**, *14*, 1800821; b) J. C. Chai, Z. H. Liu, J. J. Zhang, J. R. Sun, Z. Y. Tian, Y. Y. Ji, K. Tang, X. H. Zhou, G. L. Cui, *ACS Appl. Mater. Interfaces* **2017**, *9*, 17897–17905.
- [17] a) Y. Wang, Z. Li, Y. Hou, Z. Hao, Q. Zhang, Y. Ni, Y. Lu, Z. Yan, K. Zhang, Q. Zhao, F. Li, J. Chen, *Chem. Soc. Rev.* **2023**, *52*, 2713–2763; b) G. Zhang, J. Chang, L. Wang, J. Li, C. Wang, R. Wang, G. Shi, K. Yu, W. Huang, H. Zheng, T. Wu, Y. Deng, J. Lu, *Nat. Commun.* **2023**, *14*, 1081.
- [18] J. Wu, X. Wang, Q. Liu, S. Wang, D. Zhou, F. Kang, D. Shanmukaraj, M. Armand, T. Rojo, B. Li, G. Wang, *Nat. Commun.* **2021**, *12*, 5746.
- [19] Z. Piao, H. R. Ren, G. Lu, K. Jia, J. Tan, X. Wu, Z. Zhuang, Z. Han, C. Li, R. Gao, X. Tao, G. Zhou, H. M. Cheng, *Angew. Chem. Int. Ed.* **2023**, *62*, e202300966.
- [20] Z. Wang, C. Chen, D. Wang, Y. Zhu, B. Zhang, *Angew. Chem. Int. Ed.* **2023**, *62*, e202303950.
- [21] Z. Ren, H. Qiu, C. Fan, S. Zhang, Q. Zhang, Y. Ma, L. Qiao, S. Wang, G. Xu, Z. Cui, G. Cui, *Adv. Funct. Mater.* **2023**, *33*, 2302411.
- [22] a) Y. Wu, X. Feng, M. Yang, C. Z. Zhao, X. Liu, D. Ren, Z. Ma, L. Lu, L. Wang, G. L. Xu, X. He, K. Amine, M. Ouyang, *Adv. Sci.* **2022**, *9*, e2204059; b) J. Liu, M. Wu, X. Li, D. Wu, H. Wang, J. Huang, J. Ma, *Adv. Energy Mater.* **2023**, *13*, 2300084.
- [23] D. Zhang, M. Liu, J. Ma, K. Yang, Z. Chen, K. Li, C. Zhang, Y. Wei, M. Zhou, P. Wang, Y. He, W. Lv, Q.-H. Yang, F. Kang, Y.-B. He, *Nat. Commun.* **2022**, *13*, 6966.
- [24] K. Huang, S. Bi, B. Kurt, C. Xu, L. Wu, Z. Li, G. Feng, X. Zhang, *Angew. Chem. Int. Ed.* **2021**, *60*, 19232–19240.
- [25] Z. Guo, X. Song, Q. Zhang, N. Zhan, Z. Hou, Q. Gao, Z. Liu, Z. Shen, Y. Zhao, *ACS Energy Lett.* **2022**, *7*, 569–576.
- [26] Q. Lin, Z. Wang, L. Sun, L. Liu, X. Song, D. Li, Q. Lin, Y. Xue, X. Sun, X. Gui, K. Xu, *J. Electrochem. Soc.* **2023**, *170*, 030513.
- [27] Y. Liu, H. Zou, Z. Huang, Q. Wen, J. Lai, Y. Zhang, J. Li, K. Ding, J. Wang, Y. Lan, Q. Zheng, *Energy Environ. Sci.* **2023**, *16*, 6110–6119.
- [28] R. Zhao, M. Wu, P. Jiao, X. Wang, J. Zhu, Y. Zhao, H. Zhang, K. Zhang, C. Li, Y. Ma, Y. Chen, *Nano Res.* **2023**, *16*, 6805–6814.
- [29] S. L. Cui, X. W. Wu, Y. Yang, M. F. Fei, S. Liu, G. R. Li, X. P. Gao, *ACS Energy Lett.* **2022**, *7*, 42–52.

Manuscript received: March 4, 2024

Accepted manuscript online: March 22, 2024

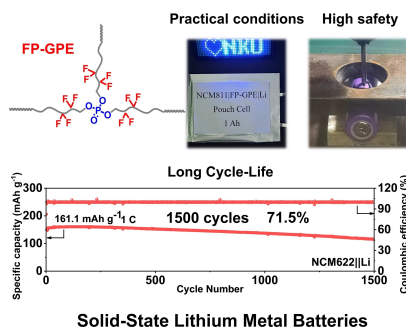
Version of record online: ■■■, ■■■

## Research Articles

## Li-Metal Batteries

N. Xu, Y. Zhao, M. Ni, J. Zhu, X. Song, X. Bi,  
J. Zhang, H. Zhang,\* Y. Ma, C. Li,  
Y. Chen\* **e202404400**

*In-Situ* Cross-linked F- and P-Containing  
Solid Polymer Electrolyte for Long-Cycling  
and High-Safety Lithium Metal Batteries  
with Various Cathode Materials



A fluorinated phosphate cross-linked gel polymer electrolyte (FP-GPE) has been designed and fabricated for high-voltage lithium metal batteries (LMBs). The FP-GPE-based batteries display excellent electrochemical performance and high safety simultaneously even at practical conditions. Moreover, the first reported solid-state 18650 cylindrical LMBs have been successfully fabricated and demonstrate exceptional safety under mechanical abuse.